Carbon cycling under 300 years of land use change: Importance of the secondary vegetation sink

Elena Shevliakova,[1] Stephen W. Pacala,[1] Sergey Malyshev,[1] George C. Hurtt,[2] P. C. D. Milly,[3] John P. Caspersen,[4] Lori T. Sentman,[5] Justin P. Fisk,[2] Christian Wirth,[6] and Cyril Crevoisier[7]

Received 30 December 2007; revised 3 November 2008; accepted 6 January 2009; published 23 June 2009.

[1] We have developed a dynamic land model (LM3V) able to simulate ecosystem dynamics and exchanges of water, energy, and CO_2 between land and atmosphere. LM3V is specifically designed to address the consequences of land use and land management changes including cropland and pasture dynamics, shifting cultivation, logging, fire, and resulting patterns of secondary regrowth. Here we analyze the behavior of LM3V, forced with the output from the Geophysical Fluid Dynamics Laboratory (GFDL) atmospheric model AM2, observed precipitation data, and four historic scenarios of land use change for 1700–2000. Our analysis suggests a net terrestrial carbon source due to land use activities from 1.1 to 1.3 GtC/a during the 1990s, where the range is due to the difference in the historic cropland distribution. This magnitude is substantially smaller than previous estimates from other models, largely due to our estimates of a secondary vegetation sink of 0.35 to 0.6 GtC/a in the 1990s and decelerating agricultural land clearing since the 1960s. For the 1990s, our estimates for the pastures' carbon flux vary from a source of 0.37 to a sink of 0.15 GtC/a, and for the croplands our model shows a carbon source of 0.6 to 0.9 GtC/a. Our process-based model suggests a smaller net deforestation source than earlier bookkeeping models because it accounts for decelerated net conversion of primary forest to agriculture and for stronger secondary vegetation regrowth in tropical regions. The overall uncertainty is likely to be higher than the range reported here because of uncertainty in the biomass recovery under changing ambient conditions, including atmospheric CO_2 concentration, nutrients availability, and climate.

Citation: Shevliakova, E., S. W. Pacala, S. Malyshev, G. C. Hurtt, P. C. D. Milly, J. P. Caspersen, L. T. Sentman, J. P. Fisk, C. Wirth, and C. Crevoisier (2009), Carbon cycling under 300 years of land use change: Importance of the secondary vegetation sink, *Global Biogeochem. Cycles*, *23*, GB2022, doi:10.1029/2007GB003176.

1. Introduction

[2] One of the most pressing challenges in the earth sciences is to understand the influence of humans on the biosphere and the global climate system. Although considerable attention has been devoted to modeling the effect of increasing atmospheric CO_2 concentration on climate and to assess ecological impacts of climate change, the potential feedbacks between the biosphere and climate are still poorly understood [*Denman et al.*, 2007]. The modeling tools needed to study complex interactions between the biosphere and climate became available only in recent decades and continue to be developed [*Friedlingstein et al.*, 2006]. The new generation of land models (e.g., IBIS [*Foley et al.*, 1996]; TRIFFID [*Cox*, 2001]; LSM-LPJ [*Bonan et al.*, 2002]; and ORCHIDEE [*Krinner et al.*, 2005]) are coupled with climate models to represent both biophysical and biogeochemical interactions and vegetation dynamics.

[3] The conversion of land from its natural state had profound effects on biogeochemical cycling and Earth climate [*Vitousek et al.*, 1997, *Houghton*, 2005]. During the last 300 years, 42–68% of the land surface has been impacted by land use activities [*Hurtt et al.*, 2006]. These land use changes are estimated to have added a net 156 GtC to the atmosphere between 1850 and 2000 [*Houghton*, 2003], altered the land surface characteristics [*DeFries et al.*, 2002a, 2002b] and affected the climate system [*Findell et al.*, 2007]. Currently, atmospheric and oceanic data imply

[1]Department of Ecology and Evolutionary Biology, Princeton University, Princeton, New Jersey, USA.
[2]Institute for the Study of Earth, Oceans, and Space, University of New Hampshire, Durham, New Hampshire, USA.
[3]U.S. Geological Survey, Princeton, New Jersey, USA.
[4]Faculty of Forestry, University of Toronto, Toronto, Ontario, Canada.
[5]Geophysical Fluid Dynamics Laboratory, NOAA, Princeton, New Jersey, USA.
[6]Max-Planck-Institute for Biogeochemistry, Jena, Germany.
[7]Laboratoire de Météorologie Dynamique, Ecole Polytechnique, IPSL, CNRS, Palaiseau, France.

0886-6236/09/2007GB003176$12.00

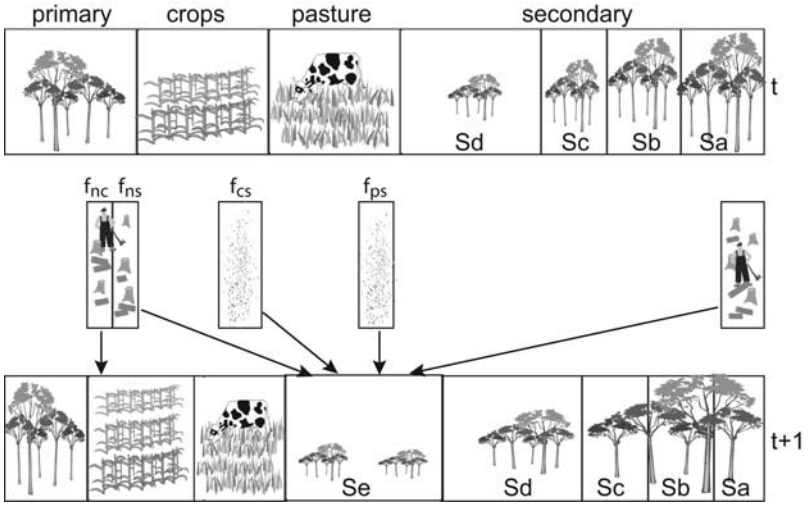

Figure 1. An example of a subgrid tile structure and land use transitions in LM3V. A fraction of natural forest f_{nc} is cleared for cropland; a fraction of natural forest f_{ns} is cut for wood harvesting and is left to regrow; a fraction of cropland f_{cs} and a fraction of pasture f_{ps} are abandoned; and a fraction of secondary forest f_{ss} is harvested for wood. After transitions, the areas of natural, cropland, pasture and secondary tiles are updated and a new secondary tiles S_e is formed.

a major unresolved terrestrial sink (~0.9–4.3 GtC/a) [*Denman et al.*, 2007]. Recent assessments showed that past land use activities contributed significantly to this sink [*SOCCR*, 2007]. Wood harvesting is particularly important because secondary forest management has significantly altered properties of land cover and created carbon sinks of hundreds Mt/a in North America, Europe, and Asia [*Pacala et al.*, 2001; *Hurtt et al.*, 2002].

[4] Previous studies estimated the global long-term flux of carbon from land use changes using either bookkeeping models [*Houghton*, 2003] or process-based ecosystem models with different cropland data sets [*McGuire et al.*, 2001; *Jain and Yang*, 2005] and regional pasture characterizations [*Jain and Yang*, 2005], and did not consider wood harvesting on primary and secondary lands. Although progress has been made at characterizing historic land use changes [*Hurtt et al.*, 2006], to our knowledge, none of the existing coupled carbon-climate models represents complex patterns of relocation of permanent agriculture (e.g., crop, pasture), shifting cultivation, logging, and the recovery of secondary (i.e., cut at least once) lands through time.

[5] In this paper, we present a new land model, LM3V, specifically developed to represent the effects of changes in land use practices on carbon cycling. The LM3V model combines functionality of a dynamic global vegetation model (DGVM) and a land surface model (LSM) and is used as a component of the GFDL Earth System Model ESM2.1. Here we describe components of the LM3V model governing vegetation dynamics, carbon cycling, and land use processes. We present results from four experiments performed in stand-alone mode, forced by four geographically explicit scenarios of land use conversion for the past 300 years [*Hurtt et al.*, 2006], together with a combination of climate data from the GFDL atmospheric model AM2 [*Anderson et al.*, 2004] and observed precipitation data [*Nijssen et al.*, 2001]. We analyze the sensitivity of carbon sources and sinks to the scenarios of land use conversion.

2. Description of LM3V

2.1. Overview of Land Cover Characterization and Model Structure

[6] LM3V tracks dynamics of natural vegetation, cropland, pastures, and secondary vegetation and is designed to be driven by scenarios of land use transitions [*Hurtt et al.*, 2006]. The model describes land cover at each grid cell as a combination of tiles in four land use categories: lands undisturbed by human activities (i.e., "primary" or "potential"), cropland, pasture, and lands harvested at least once (i.e., "secondary"), including managed forests and abandoned cropland and pasture. Primary lands, cropland and pasture are each represented by one tile per grid cell. Secondary vegetation is represented by more than one tile within a grid cell to capture the land age distribution in the cell (the distribution of times since the last harvest). Both the number and relative area of secondary tiles vary through time to model the historical legacy of past harvests (section 2.2). In the current implementation of the model, each grid cell could have from 1 to 15 tiles (12 secondary tiles, 1 crop, 1 pasture, and 1 natural vegetation tile) depending on the history of transitions (Figure 1). The model includes five vegetation types (C3 and C4 grasses, temperate deciduous, tropical, and cold evergreen trees (section 2.3)) and allows only one type of vegetation per tile. The biogeography parameterization uses the total biomass in a tile in combination with prevailing climatic conditions to determine the vegetation type.

[7] LM3V simulates the dynamics of three major carbon pools (carbon in vegetation (C_v), soil (C_s), and anthropogenic storage (C_a)) and the main flows among these three pools and the atmosphere. Carbon in vegetation is partitioned into five

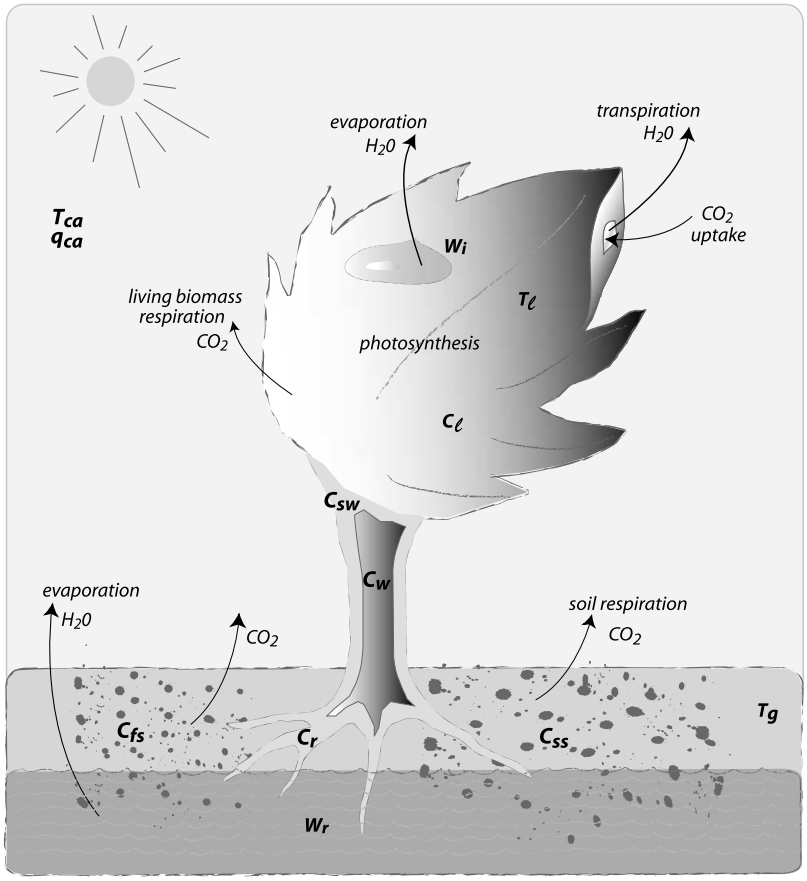

Figure 2. The LM3V coupled photosynthesis, canopy energy/moisture exchange, and soil physics/hydrology components simulate fluxes of energy, water, and CO_2 among major pools in vegetation, soil, and atmosphere on timescales of 30 min. Vegetation carbon pools (C_l, C_r, C_{sw}, C_w, and C_{vl} (not shown)) are updated daily depending on the amount of accumulated carbon and phenological state.

pools: leaves, fine roots, sapwood, heartwood (hereafter simply "wood"), and labile carbon stores (Figure 2). The sizes of the pools are modified daily depending on the amount of carbon accumulated in the biophysics model and according to a set of allocation rules (section 2.4). Additionally, the model simulates changes in the vegetation carbon pools due to phenological processes (e.g., leaf drop and display) (section 2.5) and natural mortality and fire (section 2.6). Carbon lost from vegetation pools by the above processes and during land use conversions is deposited into two soil carbon pools that differ in the rate of decomposition (section 2.7). Losses of carbon from soil pools to the atmosphere (i.e., "soil respiration") depend on the amount of stored carbon, soil temperature, and water.

[8] We distinguish three groups of parameters in LM3V depending on the method of estimation. Values in the first group were taken directly from the literature (Figure S4).[1] Values in the second group were obtained from analyses of two models with detailed representation of soil biogeochemistry [*Parton et al.*, 1992] and size-age-structured vegetation dynamics [*Moorcroft et al.*, 2001; *Hurtt et al.*, 2002] (Figure S5). Values in the third group were chosen to match characteristics of major world vegetation types using quasi-equilibrium relationships as described in sections 2.4 and 2.7 (Figures S6–S8).

2.2. Land Use Characterization

[9] In the land use component of LM3V, a historical scenario specifies annual transition rates among land use categories in each grid cell (Figure 1). Let $\vec{L}(t)$ be the vector of areas of tiles within a grid cell in year t, and $\lfloor \tau_i^j(t) \rfloor$ be the matrix of transition rates from a category i to a category j.. Then, the time evolution of a land use category j is given by:

$$dL_j(t)/dt = \sum_i \tau_i^j(t). \quad (1)$$

There is one tile per cell for croplands, pastures, and primary vegetation but several tiles for secondary vegetation to keep track of the age distribution of secondary lands. When a parcel of primary or secondary land is harvested or an agricultural parcel is abandoned, a new secondary tile is

[1] Auxiliary materials are available in the HTML. doi:10.1029/2007GB003176.

generated and its age is set to zero. To keep the number of secondary tiles from growing too large, tiles are merged if their states are sufficiently similar while preserving water, energy, and carbon balances. All parameters in the land use component are from the Miami-LU model developed by *Hurtt et al.* [2002].

[10] Every time a parcel of primary or secondary land is converted into cropland, pasture, or secondary forest, any biomass in excess of a small amount $C_0 = 0.1$ kgC/m^2 is cut. A fraction of cut sapwood and wood $f_r = 0.25$ is left as a residue and is deposited into the tile's soil carbon pool together with all leaf, root, and labile carbon. The remaining fraction of harvested sapwood and wood is collected as wood harvest. Wood harvest is partitioned among three anthropogenic wood pools characterized by turnover rates.

[11] In this study, the following two wood harvesting rules were applied: (1) primary forest is harvested before secondary forest and (2) harvest of secondary forest proceeds from the highest to the lowest biomass in a grid cell [*Hurtt et al.*, 2002]. Currently, the LM3V land use model does not account for the spatial transfers of forestry and agricultural products between different regions.

[12] Croplands and pastures are harvested annually (all annual processes are invoked at the end of the calendar year). Croplands are initialized annually with a grass vegetation type and biomass $C_0 = 0.1$ kgC/m^2. All leaf carbon in croplands and the aboveground fraction of labile carbon stores are harvested annually and released back to the atmosphere during the next year, and all remaining carbon is transferred to soil pools. On pastures a fraction of leaf carbon ($f_g = 0.25$) is grazed annually and partitioned into a livestock respiration fraction ($f_a = 0.9$) and a grazing residue fraction ($1 - f_a = 0.1$) that is returned to the soil pools. The ungrazed carbon is reallocated to rebalance leaf, roots, and labile store carbon pools. Consumed pasture carbon is released back to the atmosphere.

2.3. Plant Diversity and Biogeography

[13] The five vegetation types are combinations of three characteristics: physiology (i.e., C3 versus C4), leaf longevity (i.e., temperate versus tropical broadleaf versus cold evergreen), and allocation ratios among stems, roots, and leaves (i.e., tree versus grass). All tree vegetation types have C3 physiology. The tropical tree type can behave as evergreen or deciduous depending on the environmental conditions. LM3V does not distinguish between shrub and tree types. However, land dominated by a tree type with a low height and biomass is functionally similar to a shrub-dominated ecosystem.

[14] LM3V combines bioclimatic constraints with parameterizations derived from the ED model, which explicitly represents height-structured competition [*Moorcroft et al.*, 2001]. Once a year, the distribution of vegetation types is reevaluated on the basis of accumulated biomass and climatic conditions during the previous year. A grid cell is occupied by a grass vegetation type if its biomass density is less than 1 kgC/m^2 (on the basis of analysis of *Olson at el.* [1985]. For grass, the dominance of a specific photosynthetic pathway is defined from an empirical function $f_{c4}(T_{ave}, p_{ave})$ of average annual mean temperature T_{ave}(°K) and precipitation p_{ave}(mm/a):

$$f_{c4}(T_{ave}, p_{ave}) = \exp(-\theta_1 \cdot (\theta_2 - T_{ave}) - \theta_3 \cdot (\theta_2 - T_{ave}) \cdot p_{ave}), \tag{2}$$

where θ_1, θ_2, θ_3 are statistically estimated parameters (Figure S5). If $f_{c4}(T_{ave}, p_{ave}) > 0.5$, then a grass cell is designated to have C4 physiology, and C3 otherwise.

[15] If a grid cell experiences between 9 and 11 cold months (average canopy air temperature below 283°K), then it is assigned the cold evergreen tree type. Otherwise, the cell is classified as one of the four remaining vegetation types. If a cell contains more than 1 kgC/m^2, it is occupied by either a tropical (average canopy air temperature of the coldest month T_{cold} above 278K) or a temperate deciduous tree type; otherwise, it is occupied by either C3 or C4 grass.

2.4. Vegetation Growth and Allocation

[16] LM3V represents vegetation in terms of five carbon pools: leaves C_l, fine roots C_r, sapwood C_{sw}, labile carbon stores (including seasonally dormant root tissues) C_{vl}, and wood C_w (Figure 2). The first four pools comprise a living carbon pool. Change in the living carbon pool is computed daily as a balance between net primary production (NPP) and turnover losses:

$$\frac{dC_{liv}}{dt} = \begin{cases} \mathrm{NPP} - \alpha_l C_l - \alpha_r C_r - \alpha_{sw} C_{sw} - \mu C_{liv} & \text{during leaf-on season} \\ \mathrm{NPP} - \alpha_{sw} C_{sw} - \mu C_{liv} & \text{during leaf-off season} \end{cases} \tag{3}$$

where α_l and α_r are the turnover rates for leaves and fine roots, α_{sw} is the rate of conversion from sapwood to wood and μ is the mortality rate. There are no turnover losses associated with the labile carbon store C_{vl}. The values of α_l, α_r, and α_{sw} are summarized in Figure S4. The NPP formulation is similar to the one in the IBIS model [*Foley et al.*, 1996; *Kucharik et al.*, 2000].

[17] On a daily basis, the living carbon C_{liv} is partitioned among the four pools $x = \{l, r, vl, sw\}$ according to $C_x(h) = p_x(h) C_{liv}$, with the fractions $p_x(h)$ defined as

leaf-on season : leaf-off season :

$$p_l(h) = \frac{1}{1 + c_1 + c_2 h}, \tag{4a}$$

$$p_l(h) = 0, \tag{4b}$$

$$p_r(h) = \frac{c_1}{1 + c_1 + c_2 h}, \tag{5a}$$

$$p_r(h) = 0, \tag{5b}$$

$$p_{vl}(h) = 0, \tag{6a}$$

$$p_{vl}(h) = \frac{1 + c_1}{1 + c_1 + c_2 h}, \tag{6b}$$

and

$$p_{sw}(h) = 1 - p_l(h) - p_r(h) - p_{vl}(h) \tag{7}$$

where h is the vegetation height, c_1 is a vegetation type-specific parameter representing the ratio of root biomass and leaf biomass, and c_2 is a vegetation type-specific ratio of sapwood biomass per unit vegetation height and leaf biomass. The height h (m) is an empirical function of plant total biomass derived from the results of the age-height structured ecosystem demography model ED [*Moorcroft et al.*, 2001; *Hurtt et al.*, 2002]:

$$h(b) = h_{\max}(1 - \exp(-h_1 b)), \tag{8}$$

where $h_{\max}$ is the maximum canopy height (m), h_1 is an empirical parameter(m^2/kgC), and b is the total biomass density (kgC/m^2). Note that the equations for the fractions (equations (4)–(7)) are consistent with a "pipe" model of optimal water use, with the leaf area, sapwood cross-sectional area and root surface area balanced so they colimit water transport [*Shinozaki et al.*, 1964]. Parameters c_1 (unitless) and c_2 (1/m) were estimated from equations (9) and (10).

$$c_1 = \frac{\overline{C}_r \cdot \sigma_l}{LAI}, \tag{9}$$

$$c_2 = \frac{\overline{C}_{sw}}{\overline{h}\,\overline{C}_l} = f\sigma_l \rho_{wc} \frac{A_{sw}}{A_l}. \tag{10}$$

where $\overline{C}_r$, $\overline{C}_{sw}$ and $\overline{C}_l$ are, respectively, typical equilibrium biomass densities of fine roots, sapwood and leaves from the literature; σ_l (m^2/kgC) is the specific leaf area, f is the form factor relating the product of basal area and height to biomass, ρ_{wc} (kgC/m^3) is wood carbon density, and A_{sw}/A_l is the ratio of sapwood area to leaf area.

[18] The balance between sapwood conversion into wood and wood losses through branch fall and mortality defines the rate of change of the carbon stored in wood biomass C_w

$$\frac{dC_w}{dt} = \alpha_{sw} C_{sw} - \left(\mu + \frac{1}{\tau_f}\right) C_w, \tag{11}$$

where μ is the mortality rate (Figure S7) and τ_f is the fire return interval (section 2.6).

2.5. Phenology

[19] The phenology of deciduous plants in LM3V is governed by monthly environmental triggers and is based on the phenology model used in ED [*Moorcroft et al.*, 2001; *Hurtt et al.*, 2002]. Leaves and fine roots are dropped or become dormant when one of the two conditions is met: the mean monthly canopy air temperature drops below 10°C or the mean monthly plant-available soil water in the root zone falls to less than 10% of its maximum possible value. In the event of phenological leaf drop, a fraction $f_l = 0.5$ of leaf carbon and fine root carbon is deposited into the soil carbon pools. The remaining fraction $(1 - f_l)$ of leaf and fine root carbon is retained as labile carbon stores.

[20] Conversely, when the mean monthly temperature rises above 10°C and the mean monthly soil water is above the 10% threshold, leaves and respiring fine roots are formed from the "living" carbon pool to maintain fractions $p_l(h)$ and $p_r(h)$ defined in the previous section and labile carbon stores are set to zero. If leaves are displayed, LAI is computed as the product of the leaf carbon pool C_l and the specific leaf area σ, which is a function of leaf longevity [*Reich et al.*, 1997]. Although LM3V's treatment of phenology is very simple, the results of simulations (not shown) suggest that it captures the seasonal cycle of both drought- and cold-deciduous plants.

2.6. Disturbance

[21] The model considers two types of natural disturbance: natural mortality and fire. The effects of herbivores, extreme events, and competition are parameterized by a single constant natural mortality rate μ that varies with vegetation type (Figure S7) similar to the approach of IBIS. Mortality losses are computed annually so that carbon is decreased proportionally in leaf, root, sapwood, labile stores, and wood pools, and mortality losses are added to the soil carbon pools. Mortality rates for five vegetation types are estimated phenomenologically from the quasi-equilibrium values of net primary production (NPP_{eq}), biomass (C), and leaf and roots litter (L) available in the literature.

$$\mu = \frac{\mathrm{NPP}_{eq} - L}{C}. \tag{12}$$

[22] The second kind of disturbance is fire. Few models describe the effect of fire on vegetation in a mechanistic way [*Thonicke et al.*, 2001; *Arora and Boer*, 2005]. Most dynamical global vegetation models either do not simulate fire (e.g., TRIFFID) [*Cox*, 2001] or use very simple approaches (e.g., ED) [*Moorcroft et al.*, 2001]. In LM3V fire disturbance is simulated following the simple approach of the ED model, which has been shown to produce reasonable results in the U.S. and Brazil [*Moorcroft et al.*, 2001; *Hurtt et al.*, 2002]. Fire potential in any month is the product of a historic fire return rate ($1/\pi$) and a modulation factor proportional to fuel amount (aboveground biomass) and a drought indicator. In the present formulation, fire losses are computed once a year; the annual fire mortality rate ($1/\tau_f$) is given by:

$$\frac{1}{\tau_f} = \frac{1}{\pi} \frac{\sum_{j=1}^{12} \delta_j C_{abg_j}}{\left(\sum_{j=1}^{12} \delta_j\right) \overline{C_{abg}}}, \tag{13}$$

with

$$C_{abg_j} = C_l + f_{abg}(C_w + C_{sw} + C_{vl}) \tag{14}$$

where $C_{abg\ j}$ is the aboveground biomass in month j; f_{abg} is the fraction of wood, sapwood, and labile biomass above

ground; $\overline{C_{abg}}$ is typical equilibrium amount of aboveground biomass, and δ_j is a drought index (1 in drought months and 0 otherwise). A drought occurs when and where average monthly plant-available soil water drops below a threshold, currently set to 10% of its maximum possible value. Values of π and $\overline{C_{abg}}$ derived from published studies are given in Figure S8 for the five different vegetation types.

2.7. Soil Carbon Dynamics

[23] LM3V soil carbon dynamics is described by a highly simplified descendant of the CENTURY model [*Parton et al.*, 1987]. Carbon is represented by fast and slow decomposition stores (C_{fs} and C_{ss}), as supported by the analysis of *Bolker et al.* [1998],

$$\frac{dC_{fs}}{dt} = \upsilon_{lr}\left(\alpha_l \cdot C_l + \alpha_r \cdot C_r + L_f\right) + \upsilon_{wsw}\mu(C_{sw} + C_w) - A\left(\overline{T}_g, W_r\right) \cdot k_{fs} \cdot C_{fs} \tag{15}$$

$$\frac{dC_{ss}}{dt} = (1 - \upsilon_{wsw})\mu(C_{sw} + C_w) + (1 - \upsilon_{lr}) \cdot \left(\alpha_l \cdot C_l + \alpha_r \cdot C_r + L_f\right) - A\left(\overline{T}_g, W_r\right) \cdot k_{ss} \cdot C_{ss} \tag{16}$$

where α_l and α_r are the turnover rates for leaf and fine root pools; μ is the mortality rate for the sapwood and wood biomass pools; L_f is litter from leaves and roots; k_{fs} and k_{ss} are reference values of the soil carbon turnover rates; υ_{lr} and υ_{sws} are, respectively, the fraction of leaf and fine root litter and the fraction of sapwood and wood deposited to the fast pool; and $A(\overline{T}_g, W_r)$ is a function adopted from ED [*Moorcroft et al.*, 2001; *Linn and Doran*, 1984]. This function represents the combined effect of plant-available soil water (W_r) and soil temperature averaged over 1 m depth ($\overline{T}_g$) on microbial decomposition rates. We neglect effects of nitrogen cycling on belowground carbon.

3. Experimental Design and Analysis

3.1. Experiments and Input Data

[24] To investigate the impact of past land use transitions on the current state of the terrestrial carbon cycle, we performed an initial spinup experiment with no land use and four experiments with different scenarios of global land use history. The atmospheric CO_2 concentration was held constant at 350 ppm to eliminate any CO_2 fertilization and thus to isolate the effect of land use. All experiments were forced by a combination of atmospheric output (eight times daily) from the GFDL AM2 model (GAMDT) [*Anderson et al.*, 2004] and observed precipitation [*Nijssen et al.*, 2001]. To run long-term simulations, the data for the available period (1982–1999) were cycled several times. Note that this eliminates long-term climate trends while maintaining climate variability on scales from days to decades. The GFDL AM2 successfully simulates the current climate state (e.g., temperature, surface radiation) [*Anderson et al.*, 2004]. However, the model has precipitation biases over continents. To ameliorate the impact of these biases, we used a combination of the GFDL AGCM output (2° latitude by 2.5° longitude) with the observed precipitation data set [*Nijssen et al.*, 2001].

[25] We first simulated the global potential vegetation and soil carbon under a "no land use" assumption. The simulations began from a "cold start" for all glacier-free land cells: initial vegetation carbon density of 1 kgC/m^2, soil carbon density of 0 kgC/m^2, zero snow cover, and zero soil moisture. In this run, vegetation carbon pools equilibrated approximately after 250 years. A number of modeling studies [*Kucharik et al.*, 2000; *Hoffman et al.*, 2005] indicate that soil carbon spinup requires a much longer time (~thousands of years) than vegetation carbon (~hundreds of years). We accelerated the soil carbon spinup by substituting the long-term equilibrium soil carbon distribution for the pools $\overline{C}_{fs}$ and $\overline{C}_{ss}$ that were derived from the equilibrium distribution of litter L, sapwood and wood carbon pools, and the average decomposition function A obtained after 250 years of spinup:

$$\overline{C}_{fs} = \frac{\upsilon_{lr}L + \upsilon_{wsw}(\tau + \mu)\left(\overline{C}_{sw} + \overline{C}_w\right)}{\overline{A}\left(\overline{T}_g, W_r\right) \cdot k_{fs}}, \tag{17}$$

$$\overline{C}_{ss} = \frac{(1 - \upsilon_{lr})L + (1 - \upsilon_{wsw})(\tau + \mu)\left(\overline{C}_{sw} + \overline{C}_w\right)}{\overline{A}\left(\overline{T}_g, W_r\right) \cdot k_{ss}}. \tag{18}$$

Subsequently, the soil carbon was allowed to equilibrate for another 150 years, the final 50 years of which were used for evaluation of the model's potential vegetation and soil carbon (section 4.1). The final state of vegetation and soil carbon was used as an initial condition for the experiments with different land use scenarios, all of which begin in year 1700 and end in 2000.

[26] The *Hurtt et al.* [2006] data set provides 216 land use history reconstructions varying in the source of cropland and pasture data (SAGE) [*Ramankutty and Foley*, 1999] or HYDE [*Goldewijk*, 2001] and in their assumptions about national wood harvesting practices and patterns, the biomass density of harvested forests, residence time of agriculture, and whether or not they include national wood harvest statistics. We used four land use scenarios (LU-H1, LU-S1, LU-H2, and LU-S2) formed from either the HYDE data set or a SAGE/HYDE data hybrid with either of two sets of assumptions about land transitions. The HYDE experiments (LU-H1 and LU-H2) use the *Hurtt et al.* [2006] scenarios produced from HYDE pasture and cropland distributions. To explore implications of uncertainty in the cropland data, the SAGE experiments (LU-S1 and LU-S2) use the *Hurtt et al.* [2006] scenarios produced from a combination of SAGE estimates of cropland for 1700–1992 and HYDE pasture estimates.

[27] Experiments LU-H1 and LU-S1, which are termed "focal" after *Hurtt et al.* [2006], share a common set of assumptions concerning shifting cultivation and wood harvesting. In these experiments we applied a "minimum transitions" rule (i.e., smallest possible transitions were

required to achieve the land use state) outside the tropics and a "nonminimum transitions" (e.g., shifting cultivation) rule in the tropics (23N to 23S). Under the nonminimum transition assumption, 6.7% of croplands and pastures are abandoned annually and an equal area of new croplands and pastures are created by conversion of natural or secondary lands. Primary land was given priority for land conversion and wood harvest everywhere except in Eurasia, where secondary land was prioritized. In addition, wood harvesting from forest conversion to agriculture was not counted toward fulfilling national wood harvest demand. The spatial distribution of wood harvest gave priority to grid cells with land use, then to adjacent grid cells.

[28] To investigate the significance of shifting cultivation and wood harvesting, we used two "reduced" land use history scenarios (LU-H2 and LU-S2). Land use transitions in these scenarios differ from focal scenarios in two ways: the minimum transitions rule was applied globally, thereby eliminating shifting cultivation in the tropics; and commercial wood harvest was set to 0, thereby eliminating transitions from primary to secondary vegetation and secondary to secondary vegetation.

3.2. Analysis Framework

[29] In our analyses we focus on two interrelated variables: total ecosystem (vegetation plus soil) carbon (C_e) and net ecosystem flux (NEF); we consider both global averages and averages over land use categories. NEF is the net flux of carbon from (negative values) or into (positive values) the ecosystem. The relation between global integrals of carbon storage and NEF is given by

$$\frac{d(C_e)_{glob}}{dt} = \mathrm{NEF}_{glob}, \tag{19}$$

$$\mathrm{NEF}_{glob} = \mathrm{NEP}_{glob} - E_{fire} - \left(F_{glob} + H_{glob}\right) \tag{20}$$

where $F_{glob} + H_{glob}$ is the global transfer of biomass from the ecosystems to anthropogenic storage; the first term in this sum represents wood removed in the process of land clearance for agriculture and the second term represents wood harvesting. The NEP is the NPP minus heterotrophic respiration and E_{fire} is the loss of vegetation carbon in fires. Without land use, NEF is equivalent to [-NEE] term in the *Chapin et al.* [2006] framework.

[30] The global land area can be partitioned into areas containing each of our four categories of land, which we denote by subscripts *prim*, *scnd*, *crop*, and *past*. The relations between changes in carbon storage (or net ecosystem carbon balance (NECB) in the work of *Chapin et al.* [2006]) and NEF by land use category are not as simple as those for the global integrals because areas of transition undergo changes in carbon storage and because the transitions transfer remaining carbon among the categories. These transfers among categories do not contribute to net flux from the biosphere. At the level of a land use category, carbon storage changes include these transfers in addition to actual production and harvest. The rates of change of carbon storage by land use category are given by

$$\frac{d(C_e)_{prim}}{dt} = \left(\mathrm{NEP} - E_{fire}\right)_{prim} - H_{prim} - \sum_{j=crop,past} F^j_{prim} - \sum_{j=crop,past,scnd} \tau^j_{prim}\left(\tilde{C}_e\right)_{prim} \tag{21}$$

$$\frac{d(C_e)_{scnd}}{dt} = \sum_{i\,scnd=1}^{N\,scnd} \Big\{ \left(\mathrm{NEP} - E_{fire}\right)_{i\,scnd} - H_{i\,scnd} - \sum_{j=crop,pas,scnd} F^j_{i\,scnd} - \sum_{j=crop,past,scnd} \tau^j_{i\,scnd}\left(\tilde{C}_e\right)_{iscnd} + \sum_{j=crop,past,prim,scnd} \tau^{i\,scnd}_j \left(\tilde{C}_e\right)_j \Big\} \tag{22}$$

$$\frac{d(C_e)_{crop}}{dt} = \left(\mathrm{NEP} - E_{fire}\right)_{crop} - H_{crop} - \sum_{j=past,cscnd} \tau^j_{crop}\left(\tilde{C}_e\right)_{crop} + \sum_{j=past,scnd} \tau^{crop}_j \left(\tilde{C}_e\right)_j \tag{23}$$

$$\frac{d(C_e)_{past}}{dt} = \left(\mathrm{NEP} - E_{fire}\right)_{past} - H_{past} - \sum_{j=crop,scnd} \tau^j_{past}\left(\tilde{C}_e\right)_{past} + \sum_{j=crop,scnd} \tau^{past}_j \left(\tilde{C}_e\right)_{past} \tag{24}$$

where F^j_i is removal of carbon from the ecosystem during land clearance from vegetation category i for agriculture, H_i is harvest from category i, τ^j_i is the transition rate (equation (1)), and $(\tilde{C}_e)_j$ is ecosystem carbon storage immediately after harvest or clearance of land that had been under use j. The global NEF can be decomposed into the NEF in the four land use categories,

$$\mathrm{NEF}_{prim} = \left(\mathrm{NEP} - E_{fire}\right)_{prim} - H_{prim} \tag{25}$$

$$\mathrm{NEF}_{scnd} = \sum_{i=1,\,N\,scnd} \Big\{ \left(\mathrm{NEP} - E_{fire}\right)_i - H_i \Big\} \tag{26}$$

$$\mathrm{NEF}_{crop} = \left(\mathrm{NEP} - E_{fire}\right)_{crop} - H_{crop} - \sum_{j=prim,scnd} F^{crop}_j \tag{27}$$

$$\mathrm{NEF}_{past} = \left(\mathrm{NEP} - E_{fire}\right)_{past} - H_{past} - \sum_{j=prim,scnd} F^{past}_j \tag{28}$$

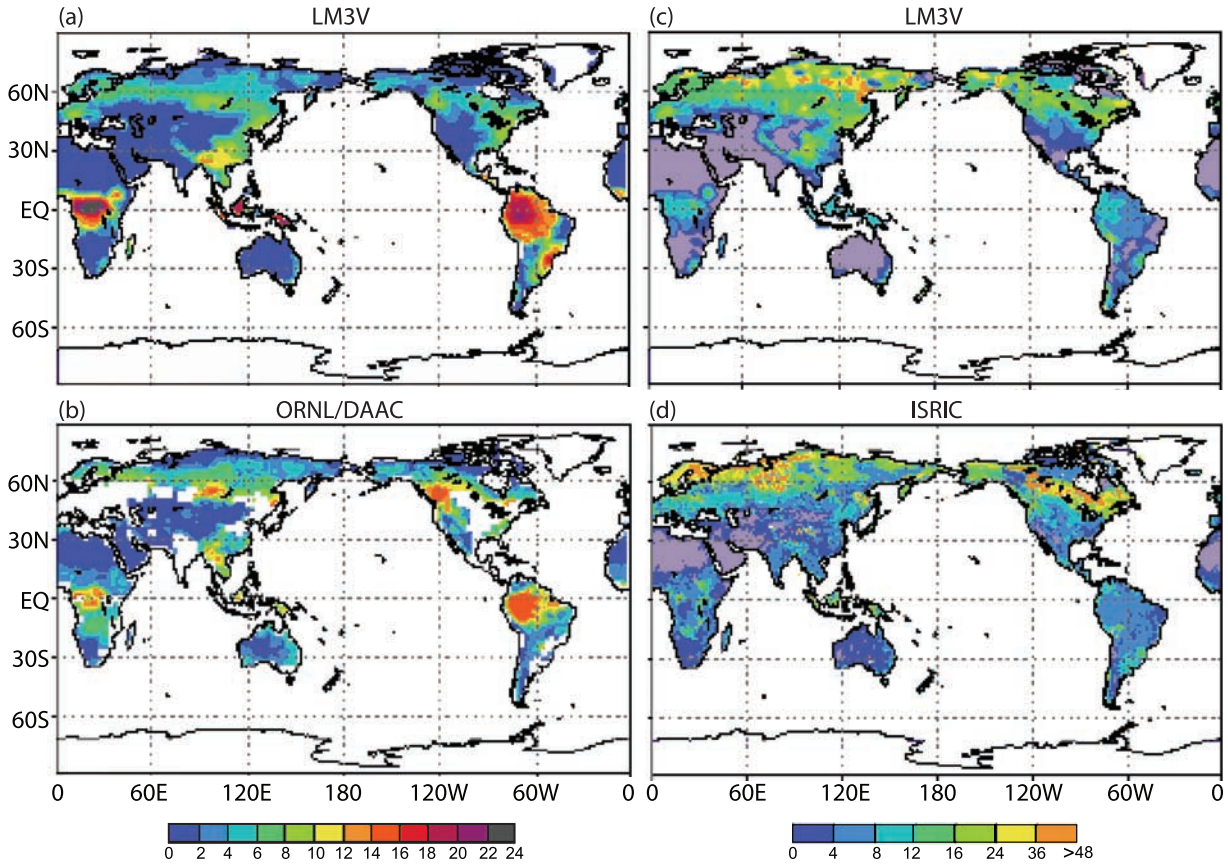

Figure 3. Distribution of (a) simulated potential vegetation biomass and (b) observed values. The observations are from the *Olson et al.* [1985] and *Gibbs* [2006] data set. The areas designated as crops or secondary vegetation in the Olson data set were excluded (Figure 3b). Distribution of (c) simulated potential and (d) observed soil carbon densities. The observed total soil carbon densities to a depth of 1 m (ISRIC data set) are shown [*Battjes*, 2002].

The change in anthropogenic storage in each pool is given by

$$\frac{d(C_{anth})_i}{dt} = \mathrm{NAF}_i = \varphi_i(F+H) - (C_{anth})_i/\tau_i \qquad (29)$$

where NAF_i and φ_i are the net anthropogenic exchange and the fraction of harvest allocated to the ith pool, τ_i is a turnover rate.

4. Results

4.1. Potential Vegetation and Soil Carbon

[31] The global total modeled equilibrium biomass is about 850 GtC, which is in the range of other DGVM simulations of 558–923 GtC [*Kucharik et al.*, 2000; *Krinner et al.*, 2005; *Sitch et al.*, 2003], and is below "prehistoric" estimates of 924–1080 GtC [*Bazilevich and Rodin*, 1971; *Adams et al.*, 1990]. We compared simulated biomass (vegetation carbon) to estimates from the data set of Major World Ecosystem Complexes Ranked by Carbon in Live Vegetation [*Olson et al.*, 1985; *Gibbs*, 2006]. To compare modeled potential vegetation to biomass distribution in the Olson database, we have excluded from the comparison all points that the Olson database designates as agricultural areas or secondary vegetation. We assume that the vegetation in the remaining categories is primarily undisturbed by human activities and is in equilibrium with the current climate. Figures 3a and 3b show comparison of the simulated global biomass distribution to the Olson distribution for the nonagricultural ecosystems with a correlation of 0.70. The range of simulated local biomass density varies from 0 kgC/m^2 in deserts to 20 kgC/m^2 in tropical rain forests.

[32] Although the biomass distribution is known reasonably well in temperate and boreal ecosystems, the tropical biomass distribution remains uncertain [*Houghton*, 2005]. We have compared above ground live biomass (AGLB) simulated by LM3V in the Amazon region to the observational data set from *Malhi et al.* [2004] for 227 old growth forests. We averaged the point observations to the LM3V grid and obtained 40 data points for comparison. Figure 4 shows that LM3V captures generally well the variation and the range of the observed AGLB with the correlation of 0.44. The spread between the data and the model predictions can be attributed to factors such as differences in the scales of observations ($\sim$1–10 km^2) and model simulations ($\sim 10^4$ km^2), climate biases in model simulations, sub-grid-scale heterogeneity in soil characteristics, and the uncer-

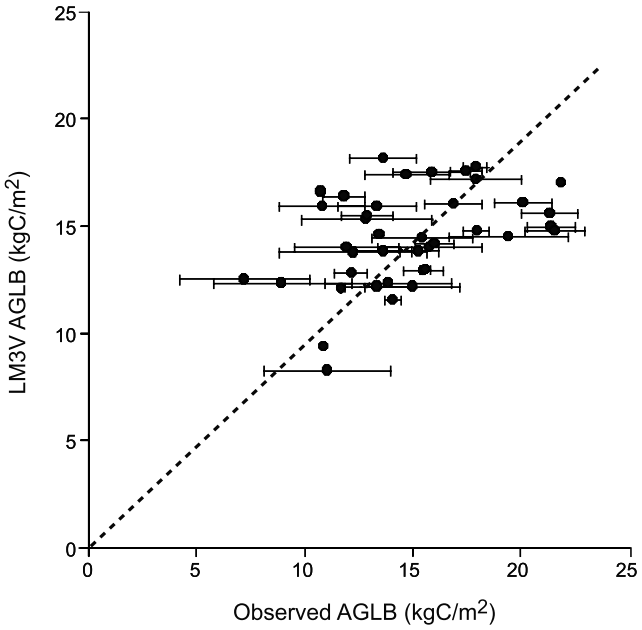

Figure 4. Comparison of simulated and observed aboveground live biomass (AGLB). The observed plot measurements [*Malhi et al.*, 2004] are averaged to the LM3V grid. Horizontal bars represent standard deviation in observations at each LM3V grid point.

tainty in the model's parameters and structure. The simulated total biomass in Amazonian natural and secondary forests is 96 GtC and is within the range of estimates reported by *Saatchi et al.* [2007] (69–102 GtC) and close to the high range of estimates reported by *Houghton et al.* [2001] (39–93 GtC).

[33] The AGLB strongly depends on the rates of aboveground wood productivity. In the Amazon region the model's values are between 0.15 and 0.4 kgC/m^{2}a, with a mean value of 0.29 kgC/m^{2}a. This estimate is within the range reported by *Malhi et al.* [2004] for 104 lowland New World old growth tropical forests (0.15 to 0.55 kgC/m^{2}a, with a mean value of 0.31 kgC/m^{2}a). The average rate of biomass accumulation in the secondary tropical forests is estimated to be 0.31 kgC/m^{2}a, although it could be strongly affected by the disturbance and the management history, particularly fire [*Chazdon et al.*, 2007]. Temperate forests are observed to have a lower wood productivity. *Jenkins et al.* [2001] estimated the wood productivity of the mid-Atlantic U.S. forests to be from 0.254 to 1.054 kg/m^{2}a (dry biomass, 2640 plots). Assuming that the aboveground wood productivity is about 80% of the total wood productivity and converting biomass to carbon (0.5 × biomass), the aboveground wood productivity is in the range from 0.10 to 0.42 kgC/m^{2}a. In the mid-Atlantic region the model's values are between 0.10 and 0.32 kgC/m^{2}a, with a mean value of 0.16 kgC/m^{2}a.

[34] The simulated global total soil organic carbon is about 1200 GtC, which is near the low end of estimates in the literature (1200–1600 GtC) [*Post et al.*, 1982; *Battjes*, 2002] and in the high end of estimates from other models (850–1200 GtC) [*Cramer et al.*, 2001]. Figures 3c and 3d show potential soil organic carbon distributions obtained from LM3V and the ISRIC data set [*Battjes*, 2002]. Because LM3V does not include a model of permafrost, the values of soil organic carbon in the high latitudes are likely to be underestimated. The local values of soil carbon vary from 0 in the desert environments to over 40 kgC/m^2 in the boreal forest, where low soil temperatures favor soil carbon accumulation.

[35] Despite the importance of NPP for the understanding of carbon dynamics, global ground NPP measurements are sporadic and scattered, and usually include only aboveground components [*Clark et al.*, 2001]. NPP data sets do not have sufficient coverage to allow a global integral. Nevertheless, the simulated global NPP of 70 GtC/a is similar to the values obtained by some DGVMs (64–74 GtC/a in the work of *Krinner et al.* [2005]; 64–70 GtC/a in the work of *Sitch et al.* [2003]) and is higher than the range of 44–66 GtC/a from the Potsdam Model Intercomparison study [*Cramer et al.*, 2001]. We made local comparisons between the LM3V equilibrium NPP and the observed site-specific values available from two data compilations. The first compilation is a combination of data from *McGuire et al.* [2002] and the data set at the Oak Ridge National Laboratory (ORNL, http://www-eosdis.ornl.gov/NPP/npp_home.html). The observed data were binned according to location (5 by 5 degree grid cells average) and observed biome type. The second compilation is the ISLSCP-2 NPP 1° × 1° data set [*Zheng et al.*, 2003], with the majority of points located in the USA; a smaller subset in Australia; and a few observations in China, Sweden, Finland and Senegal. LM3V's NPP values compare favorably with the observations of both McGuire/ORNL (r = 0.56) and ISLSCP-2 (r = 0.76) (Figure S1).

4.2. Ecosystem Carbon Storage and Fluxes Under Land Use

4.2.1. Global Carbon Storage and Net Ecosystem Flux

[36] Here we present the results of the 300-year experiments under four land use scenarios. The two experiments with focal scenarios suggest that land use activities caused substantial reduction (240 GtC for LU-H1, 294 GtC for LU-S1) in global ecosystem carbon storage during the past 300 years, with approximately 5/8 of losses from vegetation pools and 3/8 from soil pools. The two experiments with reduced land use produce a substantially smaller reduction (161 GtC for LU-H2, 210 GtC for LU-S2) of total carbon storage. The difference between the experiments with focal and reduced scenarios indicates that the effect of wood harvesting and shifting cultivation on land carbon losses is comparable in magnitude to the effect of cropland and pasture expansion. The LU-S1 scenario produces the largest carbon losses because this scenario has the highest rates of conversion from primary vegetation and because croplands account for a larger fraction of its agricultural lands than in LU-H1 (Figure 5); carbon storage in croplands is generally smaller than that in pastures (see section 4.2.2.). The largest part of the 300-year carbon loss occurs in the 20th century: losses for LU-S1,

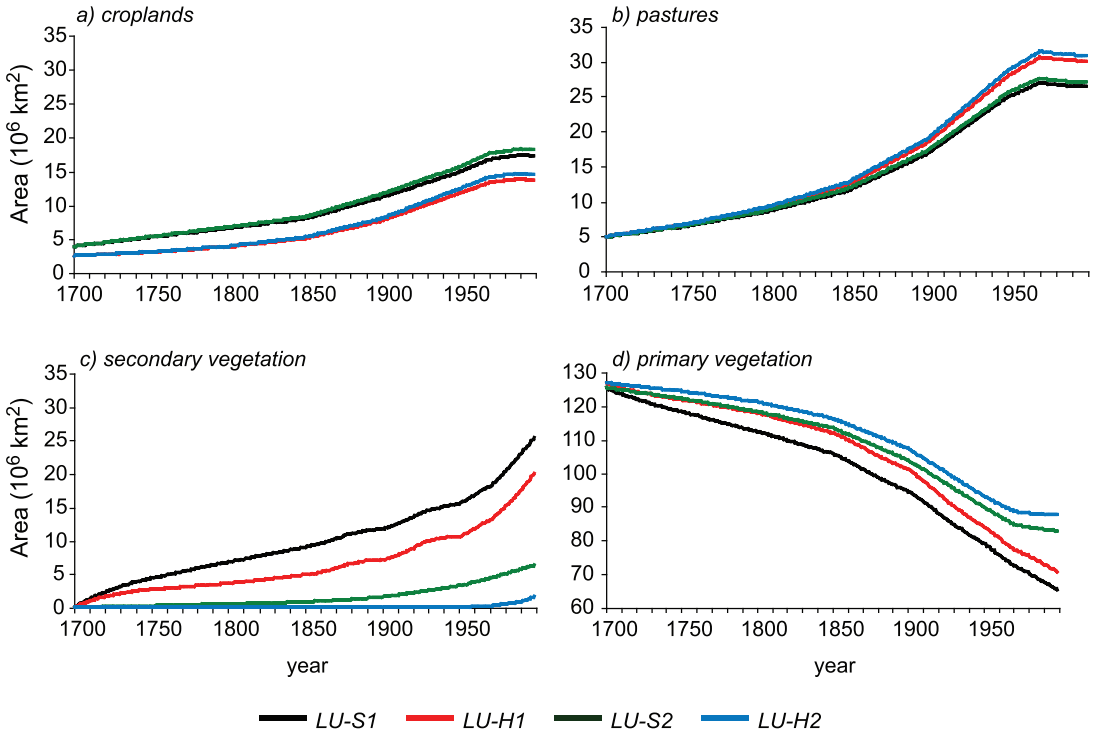

Figure 5. Land area (in 10^6 km^2) of four land use categories under different scenarios of land use change. Note that the scale for the primary vegetation area is different from the scales of other land use types.

LU-H1, LU-S2, and LU-H2 are 142, 128, 97, and 83 GtC, respectively.

[37] The evolution of global NEF under each scenario is shown in Figure 6. The global NEF dropped abruptly from near zero in the near-equilibrium segment of the model spinup (not shown) to negative values from the start of the scenario experiments. This drop corresponds to the discontinuity from natural conditions to land use management in

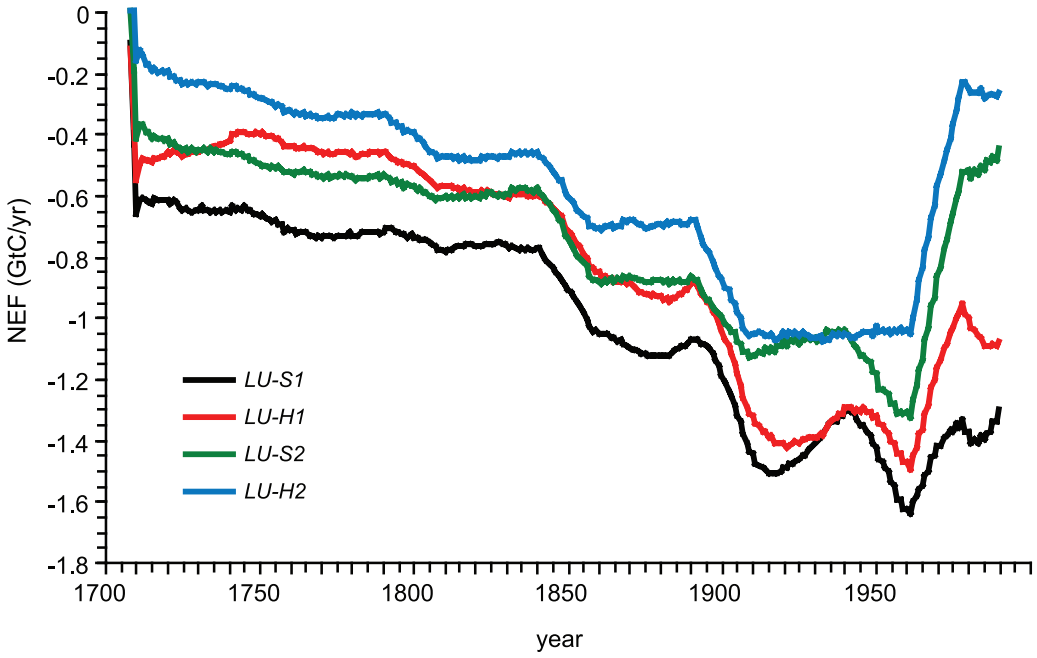

Figure 6. Global net ecosystem flux (GtC/a, 17-year running mean) simulated by the LM3v model under four different scenarios of land use change. Negative values represent losses from biosphere.

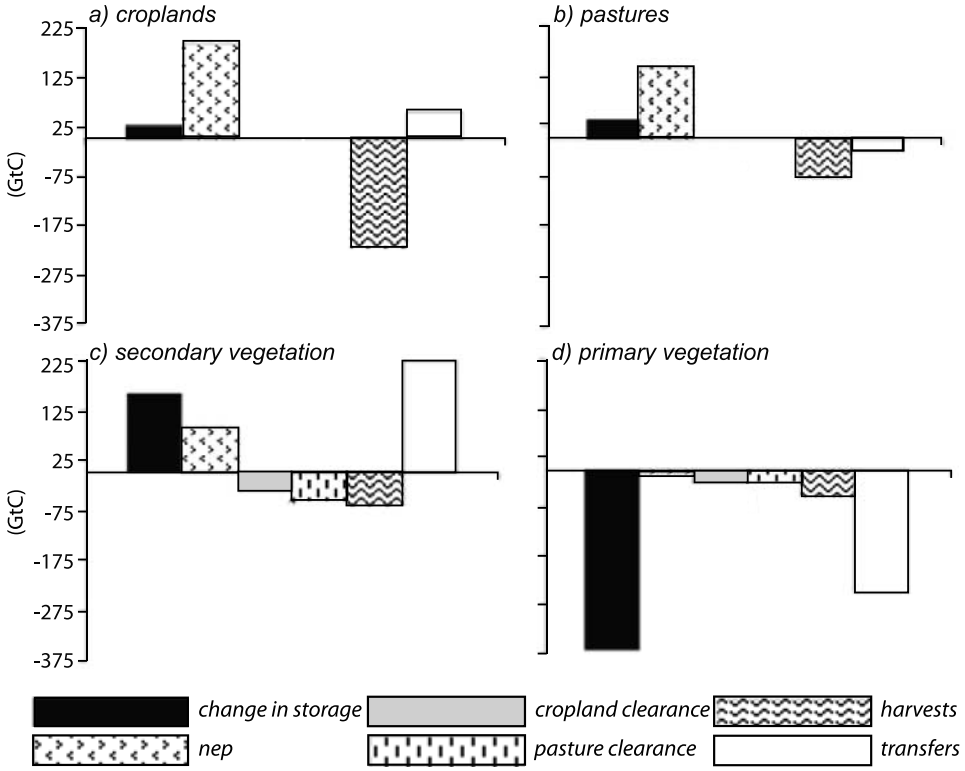

Figure 7. The cumulative 100-year carbon budget for the four land use categories for the LU-S1 experiment. A positive value represents an increase in carbon storage. Change in storage is decomposed into NEP, cropland and pasture clearance, harvests, and transfer among the land use categories.

1700 in our experiments. The 50-year periodicity in global NEF reflects a periodicity in the land use transition rates that apparently arises from temporal interpolation of the original HYDE pasture data by *Hurtt et al.* [2006]. A 17-year periodicity associated with the atmospheric forcing for the experiment has been removed by a 17-year moving average.

[38] Our results indicate that preindustrial ecosystems were not at equilibrium and land use activities created a net carbon flux from the biosphere well before 1850. As land use conversions expanded through the 18th and 19th centuries, this terrestrial flux continued to grow through the end of the 19th century. Even with the artificial 50-year signal in the experiments, it is clear that the net carbon flux from the biosphere reached a maximum during the 20th century and then abruptly began to decrease around 1960. This flux far exceeded anthropogenic storage (see section 4.3), which means that the biosphere was a source of carbon to the atmosphere. The decrease of NEF can be attributed in large part to a slowing of agricultural expansion (Figure 5). At the same time, the acceleration of harvesting of primary vegetation, which would tend to increase NEF, was partially offset by increased regrowth on secondary lands.

[39] After 1960 the net source decreased rapidly, reaching approximately 1.1 GtC/a under the LU-H1 scenario and 1.3 GtC/a under the LU-S1 scenario in the 1990s. The LU-S1 scenario produces the highest loss through almost the entire simulation period. Both focal scenarios produce larger losses than the corresponding reduced scenarios, and the differences increase rapidly after 1960 because the reduced scenarios do not include effects of wood harvesting and only account for the gross changes in pasture and croplands areas (Figure 5).

4.2.2. Changes in Carbon Storage by Land Use Category

[40] For the LU-S1 scenario, Figure 7 uses the analytic framework presented in section 3.2 to illustrate the 20th century changes (i.e., from year 1900 to year 2000) in carbon storage of each land use category along with its decomposition into (NEP $-$ E_{fire}), carbon harvests, and intercategory carbon transfers. The remainder of this section will discuss only the LU-S1 experiment. Because our experimental design contains neither CO_2 fertilization nor climate change, average (NEP $-$ E_{fire}) of primary vegetation is essentially zero. All other contributions to change of total carbon storage in primary vegetation are intrinsically negative, so primary storage decreases monotonically as primary lands undergo conversion of 30 million km^2 during the course of the 20th century (Figure 5). The 20th century loss of carbon from primary lands (370 GtC, Figure 7) is dominated by transfers of stored carbon to other land use categories (250 GtC). The estimated increase in carbon stored on secondary lands grew by 158 GtC during the 20th century. This growth was driven by carbon transfers from conversion (14 million km^2) of primary forest and abandonment of agricultural lands (222 CtC) and by regrowth (93 GtC), with these sources partially offset by harvesting and clearance for agriculture of 158 GtC.

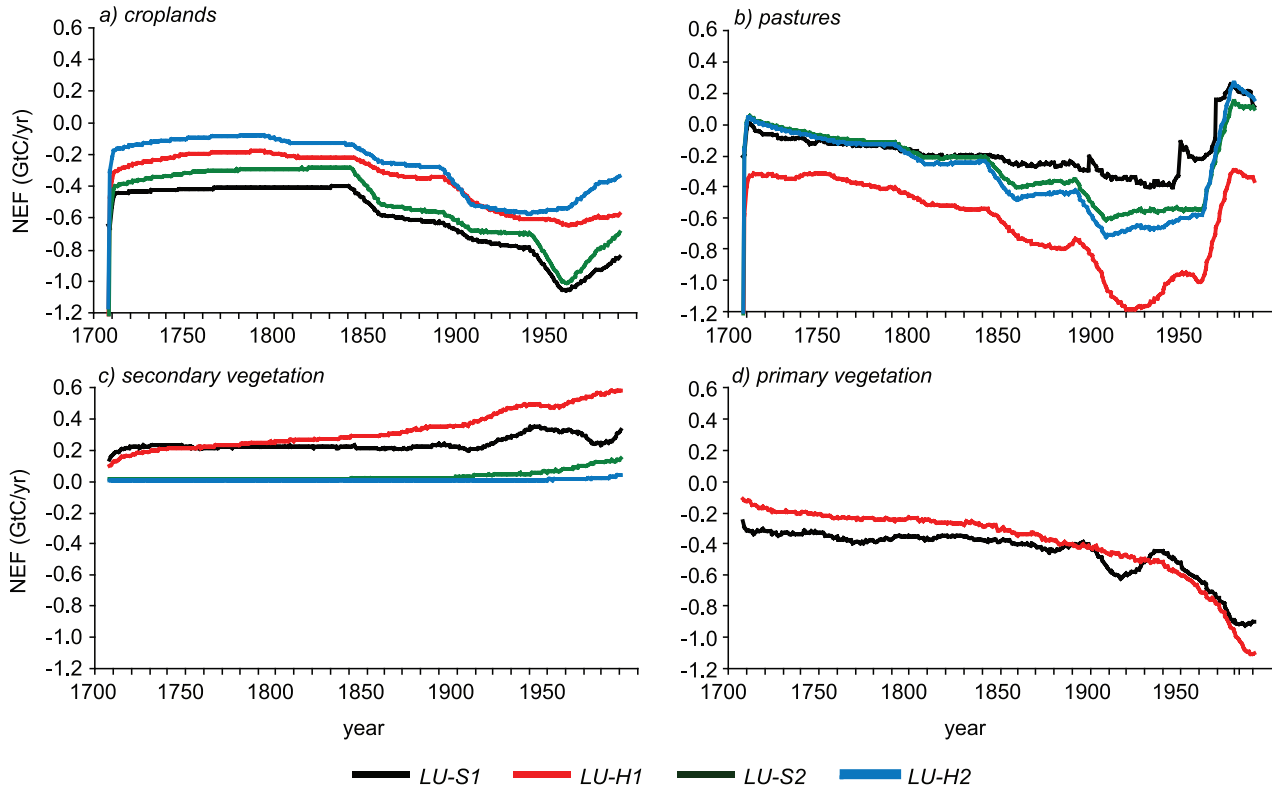

Figure 8. Net ecosystem flux (GtC/a, 17-year running mean for the four land use categories) simulated by the LM3v model under four different scenarios of land use change. Negative values represent flux from biosphere.

[41] By the end of the 20th century, agricultural lands occupied about twice as much area as secondary lands but stored almost the same amount of carbon (14% less under LU-S1). Although pasture and cropland areas grew significantly (9.7 and 6.2 million km^2, respectively), the carbon storage increased only by 39 and 28 GtC, respectively. Pasture and croplands are characterized by high (NEP $-$ E_{fire}) (142 and 195 GtC), which is offset by large harvests (77 and 220 GtC).

[42] The 20th century net transfer of carbon to croplands is positive (53 GtC), while pastures experience a net loss ($-$26 GtC). In our experiments, pastures store 2 to3 times more carbon per unit area than croplands. In pastures significant amounts of carbon are stored in soil and vegetation pools because only a fraction of aboveground carbon is removed through grazing in the model. In croplands, in contrast, all carbon in vegetation is harvested each year for agricultural consumption, so carbon storage is mainly limited to soil pools. The difference in sign of the net carbon transfers from the two agricultural land categories can be attributed at least partially to the fact that abandonment of carbon-rich pastures entails larger carbon transfers than abandonment of croplands.

4.2.3. Net Ecosystem Flux by Land Use Category

[43] Dynamics of individual land use NEFs define the evolution of the global ecosystem flux (Figure 8). In our experiments, NEFs of primary vegetation, pastures, and croplands have comparable ranges of values, but with minima at different times. Because of deceleration of agricultural expansion in the Southern Hemisphere and abandonment in the Northern Hemisphere, NEF in the focal scenarios began to decrease in magnitude from the early 20th century for pastures and from the 1960s for croplands. Under scenarios LU-H1, LU-H2, and LU-S2, pastures became a sink after 1960, reaching approximately 0.2 GtC/a in the 1990s.

[44] NEF of primary lands decreases throughout the focal simulations sharply because of continuing wood harvesting in the Northern Hemisphere and accelerating wood harvesting in the Southern Hemisphere, reaching a total of $-$1.1 GtC/a under LU-H1 and $-$0.9 GtC/a under LU-S1. There is no primary wood harvesting under the reduced land use scenarios and, therefore, no contribution from harvesting of primary lands to the global NEF. Note that by definition in LM3V, primary lands can never increase in area. If wood harvesting were to cease, primary NEF would return to zero. Primary lands can thus become a net sink only if their productivity increases because of favorable changes in climate, CO_2, or nitrogen fertilization.

[45] As Figure 8 indicates, the contribution of secondary lands to the overall NEF is qualitatively different from that of other land use types. In both hemispheres (not shown), secondary lands represent a sink of carbon under all scenarios throughout the entire length of the simulation period. The two focal scenarios produce a substantial secondary sink of up to 0.6 GtC/a (LU-H1) and 0.35 GtC/a (LU-S1), which is

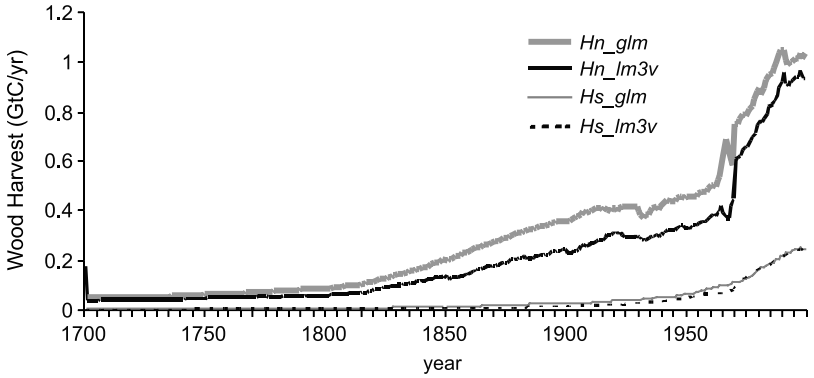

Figure 9. Annual wood harvest for the Northern (Hn) and Southern (Hs) hemispheres according to the LM3V model (lm3v) and *Hurtt et al.* [2006] reconstructions (glm).

almost entirely in the Southern Hemisphere. The higher sink under the LU-H1 scenario is partially attributable to less intense wood harvesting on secondary lands (more on primary) and partly to lower prevalence of shifting cultivation and associated clearing of secondary lands.

[46] The heterogeneity and uncertainty of land use history represented by the four scenarios produce regional differences in the distribution of carbon sources and sinks among the four experiments (Figure S2). In the 1990s, in all scenarios the biosphere generally is a carbon source where the forests have been cleared, as in Amazonia, Southeast Asia, and boreal North America and Eurasia. All scenarios suggest a tropical sink outside Amazonia, particularly in the southern part of the continent. This sink can be attributed to agricultural abandonment and secondary vegetation regrowth, particularly on pastures abandoned since the late 1970s. Additionally, a substantial sink is present in equatorial Africa under all four scenarios. Smaller areas of terrestrial uptake are scattered throughout Eurasia and North America.

[47] Although the overall patterns of NEF are similar across scenarios, some regional differences are apparent. The sink in the eastern United States is substantially higher in scenarios without wood harvesting than in the scenarios with secondary and primary vegetation harvesting. Amazonia is a stronger source under LU-S1 than under LU-S2, given the more extensive deforestation under the former.

4.3. Anthropogenic Carbon Storage and Fluxes

[48] There are three kinds of harvest in our land use model: crops collected on croplands; animal feed collected on pastures; and wood used for timber, paper and other wood products. Because we assume that crops and animal feed are consumed and respired during the same year they are harvested in, the net contribution of these two harvests to the atmospheric balance is zero. Wood and wood products, on the other hand, are allocated to three pools $(C_{anth})_i$ that are differentiated by their turnover rates: fast (τ = 1 year), medium (τ = 10 years), and slow (τ = 100 years). The same partitioning was applied everywhere in the world and wood harvests were deposited into pools at the same location where they were harvested. No attempts were made to represent a complex pattern of spatial transfers in wood and wood products. Depending on the temporal pattern of wood harvesting, use, and associated rate of release, the global anthropogenic storage pool can be either a source or sink at any given time.

[49] Figure 9 shows comparison of historic wood harvests simulated by LM3V under the LU-S1 scenario to the *Hurtt et al.* [2006] reconstruction of wood harvests. Figure 9 illustrates that wood harvesting in the Northern Hemisphere is substantially higher than wood harvesting in the Southern Hemisphere. The difference between the model and the reconstruction in the North is due to the fact that the LM3V estimate does not include wood from forests clearing for agricultural lands in Eurasia into wood harvests, although the *Hurtt et al.* [2006] estimate does. Figure 10 shows the range of global anthropogenic fluxes under two different assumptions about the partitioning of wood harvests. If only a small fraction of harvested wood is partitioned into the 100-year pool, the total NAF is relatively small compared to global NEF. For the focal scenarios, the magnitude of global NAF changes little from the preindustrial period to the end of the 20th century. To some extent, this can be attributed to the neglect of temporal trends in the uses of harvested wood. Even with a relatively large fraction of wood put into the 100-year pool, the size of the NAF sink is at most about a third of the NEF source.

5. Conclusion and Discussion

[50] In this paper we introduce a new model, LM3V, that represents a range of biophysical and biogeochemical processes in an internally consistent framework. Our study illustrates that fast and slow ecological processes, as well as impacts of land use, can be treated synchronously in the unified manner that is essential for the new generation of Earth System Models. In this paper we extended previous analyses of the global land use carbon fluxes by applying a full ecosystem model to evaluate the contribution of croplands, pastures and secondary lands.

[51] The most novel feature of LM3V is that it tracks subgrid-scale age-structured secondary vegetation resulting from changes in land use practices. To our knowledge, it is the only global model that currently represents the effects of commercial forestry, shifting cultivation, and pasture dynamics. These new features allow us to demonstrate that expansion and abandonment of pastures has as big an impact on the dynamics of carbon sources and sinks as

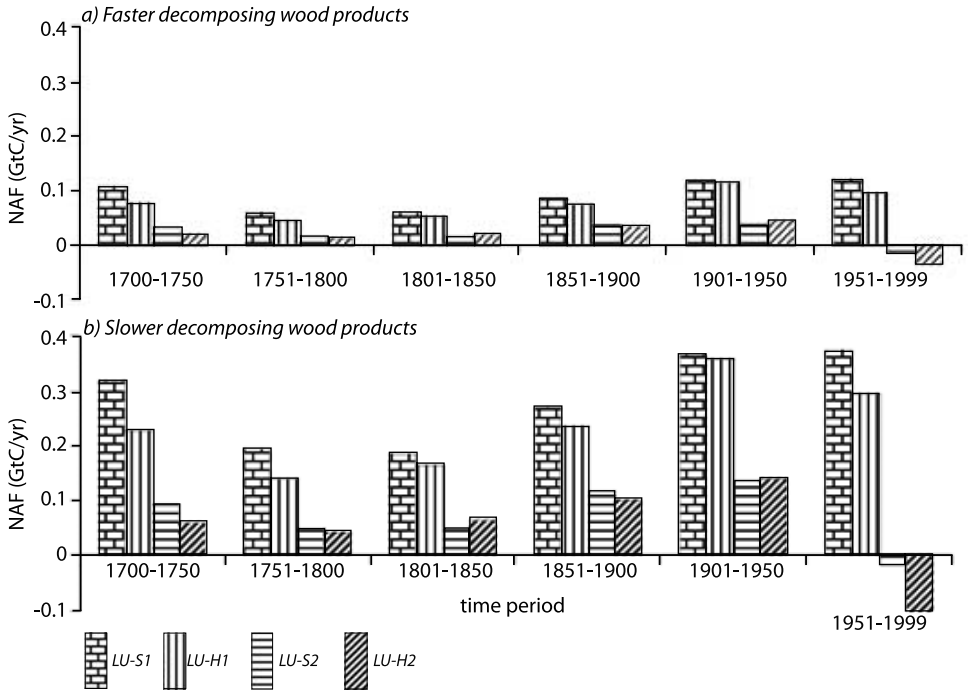

Figure 10. Mean anthropogenic pools flux under two different assumptions about harvested wood consumption and four different scenarios of land use. Positive values indicate a net storage in the anthropogenic pools, and negative values indicate net losses to the atmosphere. Under the assumption of slow decomposition, harvested wood is partitioned equally among the three wood product pools ($\varphi_i = 1/3$). Under the assumption of rapid decomposition, a fraction $\varphi_1 = 0.8$ of wood harvest is deposited into the 1-year pool, $\varphi_2 = 0.1$ is deposited into the 10-year pool, and $\varphi_3 = 0.1$ is deposited into the 100-year pool.

expansion and abandonment of croplands, which had been demonstrated in other models [*McGuire et al.*, 2001; *Jain and Yang*, 2005]. Additionally, our study shows that secondary lands are a substantial sink of carbon (0.35–0.6 GtC/a in the 1990s). To our knowledge, the only published global estimates for carbon fluxes on secondary lands stem from Houghton's bookkeeping model [*Houghton*, 1999, 2003].

[52] A recent synthesis of studies of land use change and the global carbon budget [*Denman et al.*, 2007] compared estimates from the "bookkeeping" model of *Houghton* [2003], process-driven terrestrial models [*McGuire et al.*, 2001], and studies based on remote sensing [*DeFries et al.*, 2002a, 2002b; *Achard et al.*, 2004]. The review concluded that the estimates from process-based models and remote sensing "point to a smaller source than that of *Houghton* [2003]" [*Denman et al.*, 2007, p. 518]. Our global estimate of the land use flux during the 1980s and the 1990s is consistent with the aforementioned synthesis and agrees with estimates in the lower end of the overall range.

[53] The biggest difference between our analyses and the bookkeeping model is in the estimates of the fluxes on secondary lands. Our analysis indicates a substantial secondary lands' uptake, particularly in the Southern Hemisphere, although our experiments do not produce the significant Northern Hemisphere sink indicated by previous studies (0.1–0.3 GtC/a [*Pacala et al.*, 2001; *Hurtt et al.*, 2002; *SOCCR*, 2007]). The Southern Hemisphere secondary sink of 0.3–0.6 GtC/a in the 1990s is caused by regrowth on previously harvested and abandoned agricultural lands. *Houghton*'s [2003] estimate of the tropical secondary sink is an order of magnitude smaller than ours.

[54] Our apparent Northern Hemisphere bias has a number of underlying causes. First, this study did not include the effects of fire suppression and woody encroachment. Second, the land use scenarios we used [*Hurtt et al.*, 2006] rely on country-level statistics and do not account for regional differences within the countries. The estimate of *Hurtt et al.* [2002] of the U.S. carbon sink (0.26–0.47 GtC/a for the 1980s) was derived with regional scenarios of land use, logging, and fire suppression and used different climate forcing.

[55] The relatively wide range of carbon fluxes on pastures under different scenarios (from a source of 0.37 GtC/a under LU-H1 to a sink of 0.15 GtC/a under LU-S1) appears to be caused by the differences in the area of pastures in underlying scenarios and in the intensity of shifting cultivation prescribed by these scenarios. None of our experiments produce a pasture source in the 1990s as high as the 0.48 GtC/a of *Houghton* [2003]. The small sink of 0.1–0.15 GtC/a in the 1990s due to pasture regrowth occurs mostly in the tropical regions. Our estimates are consistent with recent field studies that suggest that tropical grasslands and savannas may accumulate as much as 0.5 GtC/a [*Scurlock and Hall*, 1998].

[56] Our study, along with other studies [*McGuire et al.*, 2001; *Jain and Yang*, 2005], shows deceleration of the cropland flux since the 1960s due to agricultural abandonment. For the 1990s estimates from our model of the

cropland flux to the atmosphere with focal scenarios (0.6–0.9 GtC/a) are within the range of estimates from previously published models' estimates of 0.5–1.25 GtC/a [*McGuire et al.*, 2001]. Our results for cropland area and flux differ from those of *Houghton* [2003], who shows increase in cropland area and carbon fluxes. Our study is consistent with agriculture abandonment trends evident in the different land use and land cover data sets derived from satellite data (e.g., HYDE-2, HYDE-3 and SAGE).

[57] In LM3V, the global land use flux is similar to that of other models [*Jain and Yang*, 2005; *Houghton*, 2003] during the first half of the 20th century but smaller during the second half. Our estimates of the land use source increase only until the 1960s, when they reach values of 1.65 (LU-S1) and 1.45 (LU-H1) GtC/a and are comparable to the bookkeeping model estimates (approximately 1.85 to 1.75 in the work of *Houghton* [2003]). After the 1960s, however, the LM3V land use source declines to values of 1.1–1.3 GtC/a in the 1990s, while the bookkeeping model suggests a growing land use source reaching 2.2 ± 0.8 GtC/a [*Houghton*, 2003]. Our range of 0.2 GtC/a is due to the differences in the scenarios and the overall uncertainty is likely to be higher because of uncertainty in the biomass recovery rates which depend on availability of regeneration mechanisms and nutrients as well as the disturbance history. Furthermore, it is important to recognize that the LM3V model does not include the representation of processes such as fire suppression and woody encroachment, which are thought to decrease the magnitude of land use source further [*Pacala et al.*, 2001]. The 1 GtC/a reduction in the magnitude of the land use source relative to *Houghton*'s [2003] estimates also implies a 1 GtC/a reduction in the magnitude of the "missing sink."

[58] To build on the results of this study and extend the functionality of the model, a number of improvements are envisioned. The priority areas for further development include increase of plant functional diversity, introduction of mechanistic competition among different types of vegetation, improvement of the fire model, enhanced model of agriculture, and the addition of nitrogen and phosphorus dynamics.

[59] **Acknowledgments.** The authors are most grateful to Ronald J. Stouffer, Songmiao Fan, James Randerson, and two anonymous reviewers for their helpful comments on the manuscript. This work has been supported by the Cooperative Institute for Climate Science (CICS) under award NA17RJ262 from the National Oceanic and Atmospheric Administration (NOAA), U.S. Department of Commerce; by the Carbon Mitigation Initiative with support provided by the British Petroleum Company and the Ford Motor Company; and by a grant from the NASA Interdisciplinary Science Program. The statements, findings, conclusions, and recommendations are those of the authors and do not necessarily reflect the views of NOAA and NASA.

References

Achard, F., H. D. Eva, P. Mayaux, H.-J. Stibig, and A. Belward (2004), Improved estimates of net carbon emissions from land cover change in the tropics for the 1990s, *Global Biogeochem. Cycles*, *18*, GB2008, doi:10.1029/2003GB002142.

Adams, J. M., H. Faure, L. Faure-Denard, J. M. McGlade, and F. I. Woodward (1990), Increases in terrestrial carbon storage from the Last Glacial Maximum to the present, *Nature*, *348*, 711–714, doi:10.1038/348711a0.

Anderson, J. L., et al. (2004), The new GFDL global atmosphere and land model AM2/LM2: Evaluation with prescribed SST simulations, *J. Clim.*, *17*(24), 4641–4673, doi:10.1175/JCLI-3223.1.

Arora, V. K., and G. J. Boer (2005), Fire as an interactive component of dynamic vegetation models, *J. Geophys. Res.*, *110*, G02008, doi:10.1029/2005JG000042.

Battjes, N. H. (2002), ISRIC-WISE global dataset of derived properties 0.5 by 0.5 degree grid (version 2.0), *Rep. 2002/03*, ISRIC. Wageningen, Netherlands. (Available at http://www.iscric.org)

Bazilevich, N. I., and L. Y. Rodin (1971), Geographical regularities in productivity and the circulation of chemical elements in the Earth's main vegetation types, *Sov. Geogr. Rev. Transl.*, *12*, 24–53.

Bolker, B. M., S. W. Pacala, and W. J. Parton Jr. (1998), Linear analysis of soil decomposition: Insights from the century model, *Ecol. Appl.*, *8*(2), 425–439, doi:10.1890/1051-0761(1998)008[0425:LAOSDI]2.0.CO;2.

Bonan, G. B., K. W. Oleson, M. Vertenstein, S. Levis, X. Zeng, Y. Dai, R. E. Dickinson, and Z.-L. Yang (2002), The land surface climatology of the Community Land Model coupled to the NCAR Community Climate Model, *J. Clim.*, *15*(22), 3123–3149, doi:10.1175/1520-0442(2002)015<3123:TLSCOT>2.0.CO;2.

Chapin, F. S., III, et al. (2006), Reconciling carbon-cycle concepts, terminology, and methods, *Ecosystems (N. Y., Print)*, *9*, 1041–1050, doi:10.1007/s10021-005-0105-7.

Chazdon, R. L., S. G. Letcher, M. van Breugel, M. Martinez-Ramos, F. Bongers, and B. Finegan (2007), Rates of change in tree communities of secondary neotropical forests following major disturbances, *Philos. Trans. R. Soc. B*, *362*, 273–289, doi:10.1098/rstb.2006.1990.

Clark, D. A., S. Brown, D. Kicklighter, J. Chambers, J. R. Thomlinson, and Ni Jian (2001), Measuring net primary production in forests: Concepts and field methods, *Ecol. Appl.*, *11*, 356–370, doi:10.1890/1051-0761(2001)011[0356:MNPPIF]2.0.CO;2.

Cox, P. M. (2001), *Description of the "TRIFFID" dynamic global vegetation model*, Tech. Note *HCTN 24*, Hadley Cent, Met Office,, Berks, U. K.

Cramer, W., et al. (2001), Global response of terrestrial ecosystem structure and function to CO_2 and climate change: Results from six dynamic global vegetation models, *Global Change Biol.*, *7*, 357–373, doi:10.1046/j.1365-2486.2001.00383.x.

DeFries, R. S., L. Bounoua, and G. J. Collatz (2002a), Human modification of the landscape and surface climate in the next fifty years, *Global Change Biol.*, *8*, 438–458, doi:10.1046/j.1365-2486.2002.00483.x.

DeFries, R., R. A. Houghton, M. Hansen, C. Field, D. Skole, and J. R. G. Townshend (2002b), Carbon emissions from tropical land use change based on satellite observations for the 1980s and 90s, *Proc. Natl. Acad. Sci. U. S. A.*, *99*, 14,256–14,261, doi:10.1073/pnas.182560099.

Denman, K. L., et al. (2007), Coupling between changes in the climate system and biogeochemistry, in *Climate Change 2007: The Physical Science Basis. Contribution of Working Group I to the Fourth Assessment Report of the International Panel on Climate Change*, edited by S. Solomon et al., pp. 499–587, Cambridge Univ. Press, Cambridge, U. K.

Findell, K. L., E. Shevliakova, R. J. Stouffer, and P. C. D. Milly (2007), Modeled impact of anthropogenic land cover change on climate, *J. Clim.*, *20*(14), 3621–3634, doi:10.1175/JCLI4185.1.

Foley, J. A., C. I. Prentice, N. Ramankutty, S. Levis, D. Pollard, S. Sitch, and A. Haxeltine (1996), An integrated biosphere model of land surface processes, terrestrial carbon balance, and vegetation dynamics, *Global Biogeochem. Cycles*, *10*(4), 603–628, doi:10.1029/96GB02692.

Friedlingstein, P., et al. (2006), Climate-carbon cycle feedback analysis: Results from the (CMIP)-M-4 model intercomparison, *J. Clim.*, *19*, 3337–3353, doi:10.1175/JCLI3800.1.

Gibbs, H. K. (2006), *Olson's Major World Ecosytem Complexes Ranked by Carbon in Live Vegetation: An Updated Database Using the GLC2000 Land Cover Product*, *Rep. NDP-017b*, Carbon Dioxide Inf. Anal. Cent., Oak Ridge Natl. Lab., Oak Ridge, Tenn. (Available at http://cdiac.ornl.gov/epubs/ndp/ndp017/ndp017b.html)

Goldewijk, K. (2001), Estimating global land use change over the past 300 years: The HYDE database, *Global Biogeochem. Cycles*, *15*(2), 417–434, doi:10.1029/1999GB001232.

Hoffman, F., I. Fung, and J. John (2005), Preliminary results from the C4MIP Phase 1 simulations using the CCSM3-CLM3-CASA coupled model, *Eos Trans. AGU*, *86*(52), Fall Meet. Suppl., Abstract B33G-07.

Houghton, R. A. (1999), The annual net flux of carbon to the atmosphere from changes in land use 1850–1990, *Tellus, Ser. B*, *51*, 298–313.

Houghton, R. A. (2003), Revised estimates of the annual net flux of carbon to the atmosphere from changes in land use and land management 1850–2000, *Tellus, Ser. B*, *55*, 378–390, doi:10.1034/j.1600-0889.2003.01450.x.

Houghton, R. A. (2005), Aboveground forest biomass and the global carbon, *Global Change Biol.*, *11*, 945–958, doi:10.1111/j.1365-2486.2005.00955.x.

Houghton, R. A., K. T. Lawrence, J. L. Hackler, and S. Brown (2001), The spatial distribution of forest biomass in the Brazilian Amazon: A compar-

ison of estimates, *Global Change Biol.*, *7*, 731–746, doi:10.1046/j.1365-2486.2001.00426.x.

Hurtt, G. C., S. W. Pacala, P. R. Moorcroft, J. P. Caspersen, E. Shevliakova, R. A. Houghton, and B. Moore (2002), Projecting the future of the US carbon sink, *Proc. Natl. Acad. Sci. U. S. A.*, *99*(3), 1389–1394, doi:10.1073/pnas.012249999.

Hurtt, G. C., S. Frolking, M. G. Fearon, B. Moore III, E. Shevliakova, S. Malyshev, S. Pacala, and R. A. Houghton (2006), The underpinnings of land-use history: Three centuries of global gridded land-use transitions, wood harvest activity, and resulting secondary lands, *Global Change Biol.*, *12*(7), 1208–1229, doi:10.1111/j.1365-2486.2006.01150.x.

Jain, A. K., and X. Yang (2005), Modeling the effects of two different land cover change data sets on the carbon stocks of plants and soils in concert with CO_2 and climate change, *Global Biogeochem. Cycles*, *19*, GB2015, doi:10.1029/2004GB002349.

Jenkins, J. C., R. A. Birdsey, and Y. Pan (2001), Biomass and NPP estimation for the mid-Atlantic region (USA) using plot level inventory data, *Ecol. Appl.*, *11*(4), 1174–1193, doi:10.1890/1051-0761(2001)011[1174:BANEFT]2.0.CO;2.

Krinner, G., N. Viovy, N. de Noblet-Ducoudré, J. Ogée, J. Polcher, P. Friedlingstein, P. Ciais, S. Sitch, and I. C. Prentice (2005), A dynamic global vegetation model for studies of the coupled atmosphere-biosphere system, *Global Biogeochem. Cycles*, *19*, GB1015, doi:10.1029/2003GB002199.

Kucharik, C. J., J. A. Foley, C. Delire, V. A. Fisher, M. T. Coe, J. D. Lenters, C. Young-Molling, N. Ramankutty, J. M. Norman, and S. T. Gower (2000), Testing the performance of a dynamic global ecosystem model: Water balance, carbon balance, and vegetation structure, *Global Biogeochem. Cycles*, *14*(3), 795–825, doi:10.1029/1999GB001138.

Linn, D. M., and J. W. Doran (1984), Effect of water-filled pore space on carbon dioxide and nitrous oxide production in tilled and non-tilled soils, *Soil Sci. Soc. Am. J.*, *48*, 1267–1272.

Malhi, Y., et al. (2004), The above-ground coarse wood productivity of 104 neotropical forest plots, *Global Change Biol.*, *10*, 563–591, doi:10.1111/j.1529-8817.2003.00778.x.

McGuire, A. D., et al. (2001), Carbon balance of the terrestrial biosphere in the twentieth century: Analyses of CO_2, climate and land use effects with four process-based ecosystem models, *Global Biogeochem. Cycles*, *15*(1), 183–206, doi:10.1029/2000GB001298.

McGuire, A. D., et al. (2002), Environmental variation, vegetation distribution, carbon dynamics and water/energy exchanges, *J. Veg. Sci.*, *13*(3), 301–314.

Moorcroft, P. R., G. C. Hurtt, and S. W. Pacala (2001), A method for scaling vegetation dynamics: The ecosystem demography model (ED), *Ecol. Monogr.*, *71*(4), 557–585.

Nijssen, B., R. Schnur, and D. P. Lettenmaier (2001), Global retrospective estimation of soil moisture using the variable infiltration capacity land surface model, 1980–1993, *J. Clim.*, *14*, 1790–1808, doi:10.1175/1520-0442(2001)014<1790:GREOSM>2.0.CO;2.

Olson, J. S., J. A. Watts, and L. J. Allison (1985), *Major World Ecosystem Complexes Ranked by Carbon in Live Vegetation (NDP-017)*, Carbon Dioxide Inf. Cent., Oak Ridge Natl. Lab., Oak Ridge, Tenn.

Pacala, S. W., et al. (2001), Consistent land- and atmosphere-based U.S. carbon sink estimates, *Science*, *292*, 2316–2320, doi:10.1126/science.1057320.

Parton, W. J., J. M. O. Scurlock, C. V. Cole, and D. S. Ojima (1987), Analysis of factors controlling soil organic matter dynamics the grasslands, *Soil Sci. Soc. Am. J.*, *51*, 1173–1179.

Parton, W. J., R. McKeown, V. Kirchner, and D. Ojima (1992), *CENTURY Users' Manual*, Nat. Resour. Ecol. Lab., Colo. State Univ., Ft. Collins, Colo.

Post, W. M., W. R. Emmanuel, P. J. Zinke, and A. G. Stangenberger (1982), Soil carbon pools and world life zones, *Nature*, *298*, 156–159, doi:10.1038/298156a0.

Ramankutty, N., and J. A. Foley (1999), Estimating historical changes in global land cover: Croplands from 1700 to 1992, *Global Biogeochem. Cycles*, *13*(4), 997–1027, doi:10.1029/1999GB900046.

Reich, P. B., M. B. Walters, and D. S. Ellsworth (1997), From tropics to tundra: Global convergence in plant functioning, *Proc. Natl. Acad. Sci. U. S. A.*, *94*(25), 13,730–13,734, doi:10.1073/pnas.94.25.13730.

Saatchi, S. S., R. A. Houghton, R. C. Dos Santos Alvala, and J. V. Soares (2007), Distribution of aboveground live biomass in the Amazon basin, *Global Change Biol.*, *13*, 816–837.

Scurlock, J. M., and D. O. Hall (1998), The global carbon sink: A grassland perspective, *Global Change Biol.*, *4*, 229–233, doi:10.1046/j.1365-2486.1998.00151.x.

Shinozaki, K., K. Yoda, K. Hozumi, and T. Kira (1964), A quantitative analysis of plant form: The pipe model theory I, *Jpn. J. Ecol.*, *14*, 97–105.

Sitch, S., et al. (2003), Evaluation of ecosystem dynamics, plant geography and terrestrial cycling in the LPJ dynamic global vegetation model, *Global Change Biol.*, *9*, 161–185, doi:10.1046/j.1365-2486.2003.00569.x.

SOCCR (2007), *The First State of the Carbon Cycle Report (SOCCR): The North American Carbon Budget and Implications for the Global Carbon Cycle. A Report by the U.S. Climate Change Science Program and the Subcommittee on Global Change Research*, edited by A. W. King et al., 242 pp., NOAA, NCDC,, Asheville, N. C.

Thonicke, K., S. Venevsky, S. Sitch, and W. Cramer (2001), The role of fire disturbance for global vegetation dynamics: Coupling fire into a dynamic global vegetation model, *Glob. Ecol. Biogeogr.*, *10*(6), 661–677, doi:10.1046/j.1466-822x.2001.00175.x.

Vitousek, P., H. Mooney, J. Lubchenco, and J. Melillo (1997), Human domination of Earth's ecosystems, *Science*, *277*, 494–499, doi:10.1126/science.277.5325.494.

Zheng, D., S. Prince, and R. Wright (2003), Terrestrial net primary production estimates for 0.5° grid cells from field observations: A contribution to global biogeochemical modeling, *Global Change Biol.*, *9*(1), 46–64, doi:10.1046/j.1365-2486.2003.00534.x.

J. P. Caspersen, Faculty of Forestry, University of Toronto, Toronto, ON M5S 3B3, Canada.

C. Crevoisier, Laboratoire de Météorologie Dynamique, Ecole Polytechnique, IPSL, CNRS, F-91128 Palaiseau CEDEX, France.

J. P. Fisk and G. C. Hurtt, Institute for the Study of Earth, Oceans, and Space, University of New Hampshire, Durham, NH 03824, USA.

S. Malyshev, S. W. Pacala, and E. Shevliakova, Department of Ecology and Evolutionary Biology, Princeton University, Princeton, NJ 08542, USA. (elena@princeton.edu)

P. C. D. Milly, U.S. Geological Survey, Princeton, NJ 08540, USA.

L. T. Sentman, Geophysical Fluid Dynamics Laboratory, NOAA, Princeton, NJ 08540, USA.

C. Wirth, Max-Planck-Institute for Biogeochemistry, Jena D-07701, Germany.